Improvements of Scintillation Modelling from Radiosonde Observations in the Arctic Region

Florian Quatresooz[1], Martin Rytir[2], Danielle Vanhoenacker-Janvier[1], Claude Oestges[1]
[1]ICTEAM, Université catholique de Louvain, Louvain-la-Neuve, Belgium, florian.quatresooz@uclouvain.be
[2]Norwegian Defence Research Establishment, FFI, N-2027 Kjeller, Norway, Martin.Rytir@ffi.no

***Abstract*—Satellite-to-ground communications at radio-frequencies above 10 GHz and low elevation angles suffer from increased scintillation. Hence, accurate modelling of this effect is required for the design and operation of those communication links. This work presents two new models for predicting the long-term scintillation standard deviation. They are based on radiosonde observations and vertical profiles of the refractive index structure parameter. Comparisons between the models and one year of scintillation measurements in Norway show good correlations and excellent agreement in terms of statistical distributions. They also enable physical insights about the seasonality observed in the measurements.**

***Index Terms*—atmospheric propagation, scintillation, satellite communications, measurements, radiosondes.**

I. Introduction

Atmospheric turbulence, especially in the troposphere, causes phase and amplitude fluctuations of satellite-to-ground communication signals. This phenomenon, referred to as scintillation, increases with the frequency and the propagation path through the atmosphere [1]. Consequently, communication links using radio-frequencies higher than 10 GHz (or even optical frequencies), as well as with low elevation angles, suffer from increased scintillation that must be mitigated.

In order to model short-term signal fades or enhancements caused by scintillation, most literature models rely on the long-term standard deviation (resp. variance) of the log-amplitude σ_χ (resp. σ_χ^2), also named scintillation standard deviation (resp. variance) in the following. Indeed, from σ_χ, probability distributions of amplitude scintillation can be obtained using the Karasawa [2], van de Kamp [3], or the ITU-R [4] models for example. They assume that the distribution of log-amplitude scintillation χ in dB, which probability density function (PDF) is $p(\chi)$, can be obtained from [3]

$$p(\chi) = \int_0^\infty p(\chi|\sigma_\chi)\ p(\sigma_\chi)\ \mathrm{d}\sigma_\chi, \tag{1}$$

where $p(\sigma_\chi)$ is the PDF of the long-term scintillation standard deviation, and $p(\chi|\sigma_\chi)$ is the PDF of χ knowing σ_χ, that is generally assumed to be Gaussian and for which expressions can be found in [2], [3].

Modelling of the scintillation standard deviation σ_χ is usually achieved by means of empirical models involving the surface wet refractivity N_{wet} [2]–[5], or other surface meteorological quantities [1]. Alternatively, models based on the vertical profile of the refractive index structure parameter C_n^2 have also been presented in the literature [6], [7]. This is the approach followed in this work, making use of a C_n^2 profile model based on its statistical definition [8]. The model rely on high-density radiosonde observations and has been previously validated for optical frequencies. This work aims at assessing its performance for radio-frequencies, extending the preliminary results in [9].

The model validation is conducted using one-year scintillation measurements in the Arctic region from a satellite beacon at 19.68 GHz. Those measurements have been presented in [10], and simultaneous radiosonde observations are available at the time of the measurements.

Section II presents the scintillation and meteorological measurements. Then, Section III describes the σ_χ models used in this work. The application of those models to the scintillation measurements is presented in Section IV, and discussed in Section V.

II. Measurements at Bjørnøya (Norway)

Meteorological observations and attenuation measurements have been collected at Bjørnøya, between May 2016 and April 2017. Bjørnøya is a small island (14 km $\times$ 17 km) located in the Barents Sea, North of continental Norway. It is equipped with a regular radiosounding station in latitude 74.5°N, longitude 19.0°E, at an altitude of 10 meters. During the attenuation measurement campaign, a receiver antenna for Ka-band was located close to the radiosounding station [10].

A. Scintillation measurements

Attenuation time series have been obtained at Bjørnøya from a 19.68 GHz beacon transmitted by the Eutelsat Ka-Sat satellite. The elevation angle was 6.6°, with the path towards the satellite going from the North of the island to its South. The receiver used an antenna of 1.2 m in diameter, and recorded data with a sampling rate of 10 samples/s. More details about the hardware used and the experiments can be found in [10].

From the attenuation data, scintillation time series have been extracted by isolating the high-frequency content using a 6$^{\text{th}}$ order Butterworth filter [11]. The chosen cut-off frequency was 2 mHz during clear-sky, and 7 mHz during rain events.

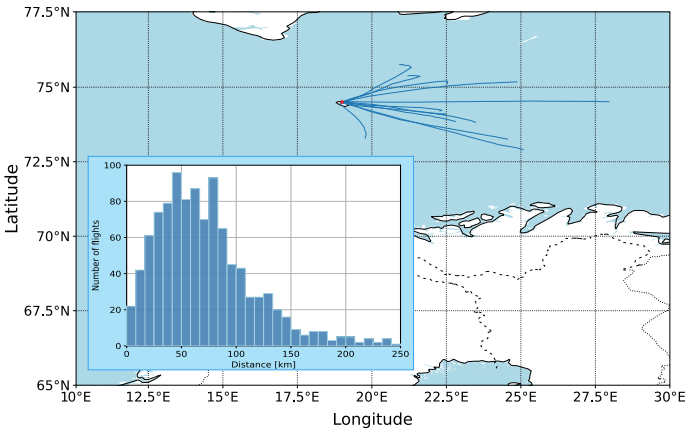

Fig. 1: Bjørnøya location and illustration of radiosonde drifting - examples and histogram of distances travelled.

The scintillation data availability over the studied 1-year period is 95.1% [10].

B. Radiosonde observations

Bjørnøya radiosonde observations are publicly available on the Norwegian Meteorological Institute website[1]. The station (ID 01028) is equipped with high-density radiosondes, measuring vertical profiles of pressure, temperature, wind speed and direction, and relative humidity. Measurements are recorded with an average vertical resolution of 10 meters, from the ground up to 25 to 30 km of altitude. During summer (approximately from April to September), radiosondes are launched twice a day, close to 00:00 UTC and 12:00 UTC. In winter (from October to March), observations are collected every 6 hours, at 00:00 UTC, 06:00 UTC, 12:00 UTC, and 18:00 UTC. In total, 1036 flights are available between May 2016 and April 2017. After discarding 9 flights associated to rainy conditions (measured rain rate larger than 2 mm/hr at launch time) and flights when no scintillation data have been collected, 1000 flights remain for further processing.

Figure 1 shows the location of Bjørnøya, depicted by the red dot. The continuous blue lines illustrate some of the radiosonde trajectories, influenced by the wind. For illustration purpose, only the furthest radiosonde travels for each month between May 2016 and April 2017 have been represented. The inset shows the histogram for all distances travelled by the radiosondes during the year of data collection. Such horizontal displacement by the radiosondes is called radiosonde drifting, and its impact on the presented scintillation model is discussed in Section V.

[1]https://thredds.met.no/thredds/catalog/remotesensingradiosonde/catalog.html, last accessed on August 18, 2023.

III. Modelling of Scintillation Standard Deviation

Scintillation arises from fluctuations of the atmospheric refractive index n along the propagation path. For radio-frequencies, the refractivity $N = 10^6(n-1)$ is given by [12]

$$N = \frac{77.6\ p}{T} + \underbrace{3.75 \times 10^5 \frac{e}{T^2}}_{N_{\text{wet}}}, \qquad (2)$$

where p is the pressure in hPa, e is the water vapour pressure in hPa, and T is the temperature in K. Equation (2) is an approximation of a more general expression that can be found in [12], [13], often used for practical works. With this approximation, the second term in (2) is associated to the wet refractivity, denoted N_{wet}.

Both models presented below make use of N (n) and/or N_{wet} in order to predict the scintillation standard deviation σ_χ.

A. Empirical model based on N_{wet}

Empirical measurements showed that the scintillation standard deviation is well correlated to the wet refractivity at the surface, denoted $N_{\text{wet,s}}$ [4], [10]. This led to several models of the form

$$\sigma_\chi = (a + b\ N_{\text{wet,s}})\, f^c g(D_e) / \sin^d(\theta) \qquad [\text{dB}], \qquad (3)$$

with f the frequency in GHz and θ the elevation angle in degrees. The coefficients a, b, c, and d, have theoretical or empirical origins and depend on the model, e.g., Karasawa [2], van de Kamp [3], or ITU-R [4]. In this work, the coefficients computed from Bjørnøya data and other measurements in Arctic conditions are used, i.e., $a = 0.8 \times 10^{-3}$ and $b = 0.91 \times 10^{-4}$ [10], with the ITU-R values for $c = 7/12$ and $d = 1.2$ [4]. The antenna aperture averaging function $g(D_e)$ is computed from [4], with D_e the effective antenna diameter.

The surface wet refractivity $N_{\text{wet,s}}$ is computed from the definition of N_{wet} in (2), using the meteorological quantities measured by the radiosonde at their first level (less than 10 m above the ground). The conversion between the relative humidity, measured by the radiosondes, and the water vapour pressure e, needed in (2), is done according to [13].

In the following, this model, making use of (3), is referred to as the N_{wet} *model*. It has initially been developed to provide long-term statistics [4], [10], even though this work also assesses its performance for instantaneous σ_χ (see Section IV).

B. C_n^2-based approach

Alternatively, the scintillation variance $[\text{dB}^2]$ can be computed from the vertical profile of the refractive index structure parameter $C_n^2(z)$ using [6], [14]

$$\sigma_\chi^2 = 42.48\ g^2(D_e)\ \frac{k^{7/6}}{(\sin(\theta))^{11/6}} \int_{\text{height}} C_n^2(z) z^{5/6}\ \text{d}z, \qquad (4)$$

where $k = \frac{2\pi}{\lambda}$ with λ the wavelength and z is the altitude above ground. The same antenna aperture averaging function as in Section III-A has been included in (4).

Several C_n^2 profile models are available in the literature, but the aim of this work is to validate the model presented in [8], [9], that relies on high-density radiosonde measurements. Using the measured vertical profiles of meteorological quantities, a vertical profile of the refractive index n is computed from (2). Then, the C_n^2 statistical definition in the inertial range enables to estimate it from the refractive index fluctuations n' between two points, located in $\boldsymbol{r}$ and $\boldsymbol{r}+\boldsymbol{\rho}$, i.e., [9]

$$C_n^2 = \frac{\left\langle \left(n'(\boldsymbol{r}+\boldsymbol{\rho}) - n'(\boldsymbol{r})\right)^2 \right\rangle}{\rho^{2/3}}, \tag{5}$$

where $\langle\cdot\rangle$ denotes an ensemble average, and ρ is the distance separating the two points where n' is evaluated.

Equation (5) is based on Kolmogorov theory of turbulence, and assumes isotropy and local homogeneity [14], [15]. For practical use, the ensemble average in (5) is substituted by a spatial three-points average, along the vertical profile. A multiplicative calibration factor has also been suggested in [8], [9]. Two different calibrations are studied for Bjørnøya data:

- A constant factor γ, determined empirically as the average of the ratios between the measured and modelled σ_χ. This leads to the so-called C_n^2 *model* for σ_χ, where σ_χ is estimated from the square-root of (4), multiplied by γ.
- A $N_{\text{wet,s}}$-dependent calibration factor, i.e., $\alpha + \beta N_{\text{wet,s}}$, inspired from the N_{wet} model in Section III-A. The coefficients α and β are obtained by computing the best polynomial fit (according to the least squares criterion) between the monthly averages of $N_{\text{wet,s}}$ and the monthly averages of the ratios between the measured and modelled σ_χ. This version of the C_n^2 model is referred to as the $C_n^2 + N_{wet}$ *model*, where the square-root of (4) is multiplied by $\alpha + \beta N_{\text{wet,s}}$ to estimate σ_χ.

The coefficients α, β, γ ensuring the best fits between the measured and modelled σ_χ for Bjørnøya data are: $\alpha = 4.75$, $\beta = -0.05$, $\gamma = 3.16$.

IV. Application to Bjørnøya Measurements

The application of the three σ_χ models described in Section III to Bjørnøya data is presented in Figure 2, showing the monthly-averaged σ_χ and surface $N_{\text{wet,s}}$. Since modelled scintillation standard deviations are only available at the times of the radiosonde launch, only the measurements collected in the one-hour window centred on the radiosonde launch have been considered. This explains why the blue curve presented in Figure 2 is slightly different from the results presented in [10], where all measurements at Bjørnøya are taken into account, and not only the ones close to the radiosonde launches.

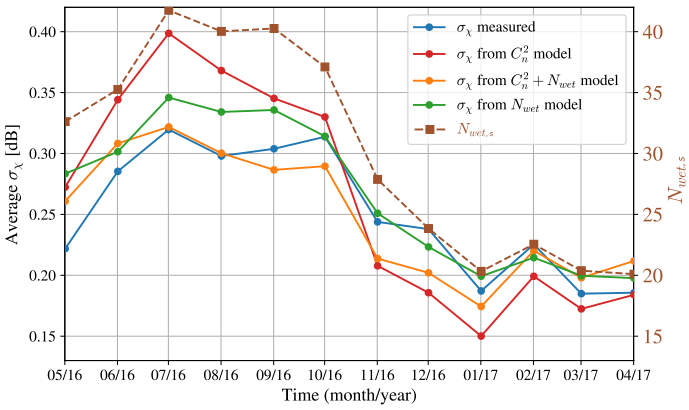

Fig. 2: Monthly averaged σ_χ and surface $N_{\text{wet,s}}$.

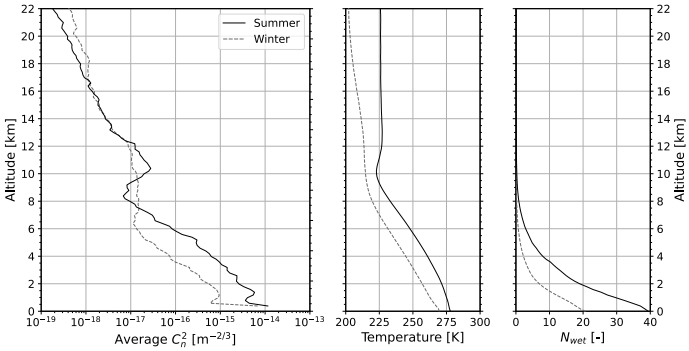

Fig. 3: Average C_n^2, temperature, and wet refractivity profiles at Bjørnøya for winter and summer months.

In Figure 2, all three models show similar performance and are able to identify the seasonal variations of the monthly-averaged σ_χ. This is particularly the case for the N_{wet} and $C_n^2 + N_{\text{wet}}$ models, and is justified by the linear dependency of those models with $N_{\text{wet,s}}$, that has a similar seasonal variation as σ_χ (see brown dashed curve in Figure 2, associated to the y-axis on the right).

Figure 3 further explains the seasonal behaviour of the C_n^2 and $C_n^2 + N_{\text{wet}}$ models, by showing the average C_n^2 profile computed from the radiosonde observations, for winter months (chosen as December, January, February, March) and for summer months (June, July, August, September). The associated average temperature and N_{wet} profiles are also depicted. A peak in the average summer C_n^2 profile can be seen at the tropopause altitude ($\sim$10 km), associated to a temperature inversion. Most discrepancies between winter and summer C_n^2 profiles are located in the troposphere (below $\sim$10 km), and tend to be associated to variations in the N_{wet} profile with the seasons. Indeed, larger N_{wet} in summer leads to larger C_n^2 values, hence increasing σ_χ.

Cumulative distributions of measured and modelled σ_χ values, for the whole year, are reported in Figure 4. They show that realistic σ_χ values are predicted by the models, in comparison with the measured ones. The agreement is

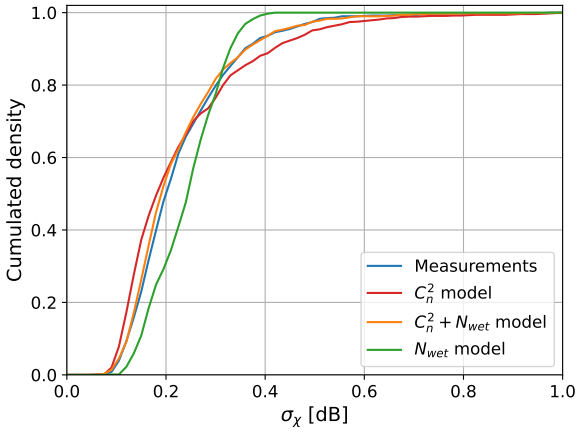

Fig. 4: Cumulative distributions of σ_χ.

TABLE I: Correlation coefficients and RMSE for all models.

	N_{wet} model	C_n^2 model	$C_n^2 + N_{\text{wet}}$ model
Correlation coefficient	0.50	0.67	0.61
RMSE [dB]	0.095	0.104	0.096

excellent for the $C_n^2 + N_{\text{wet}}$ model, while the N_{wet} model tends to give σ_χ in a short range of values, overestimating small measured σ_χ and underestimating large measured σ_χ.

This last observation can be further observed in Figure 5, giving the correlation plots between modelled and measured σ_χ. The information presented in this plot goes further than the distributions, as it takes into account the temporal accuracy of the models, i.e., their ability to give σ_χ values in agreement with the measurements at a particular instant. It shows that σ_χ from the C_n^2 and $C_n^2 + N_{\text{wet}}$ models follow the correlation line, with a larger spread for large σ_χ. The N_{wet} model is further from the correlation line. This can be expected since this model is designed to predict monthly and long-term statistics, and not instantaneous hourly averages [4], [10].

Finally, the correlation coefficients and the root-mean-square errors (RMSE) between each of the three models and the measurements are given in Table I. The best correlation with measurements is achieved with the C_n^2 model, even though it also has the largest RMSE, owing to some large outliers values.

V. Discussion

Both new σ_χ models presented in this work, i.e., the C_n^2 model and the $C_n^2 + N_{\text{wet}}$ model, are based on the estimation of C_n^2 vertical profiles. Those profiles are derived from radiosonde measurements and it is rather unlikely that they are obtained exactly along the propagation path between the satellite and the ground station. This is particularly true owing to the radiosonde drifting, introduced in Section II-B. Hence, the models presented in Section III-B assume that C_n^2 vertical profiles are relatively constant in the surrounding geographical

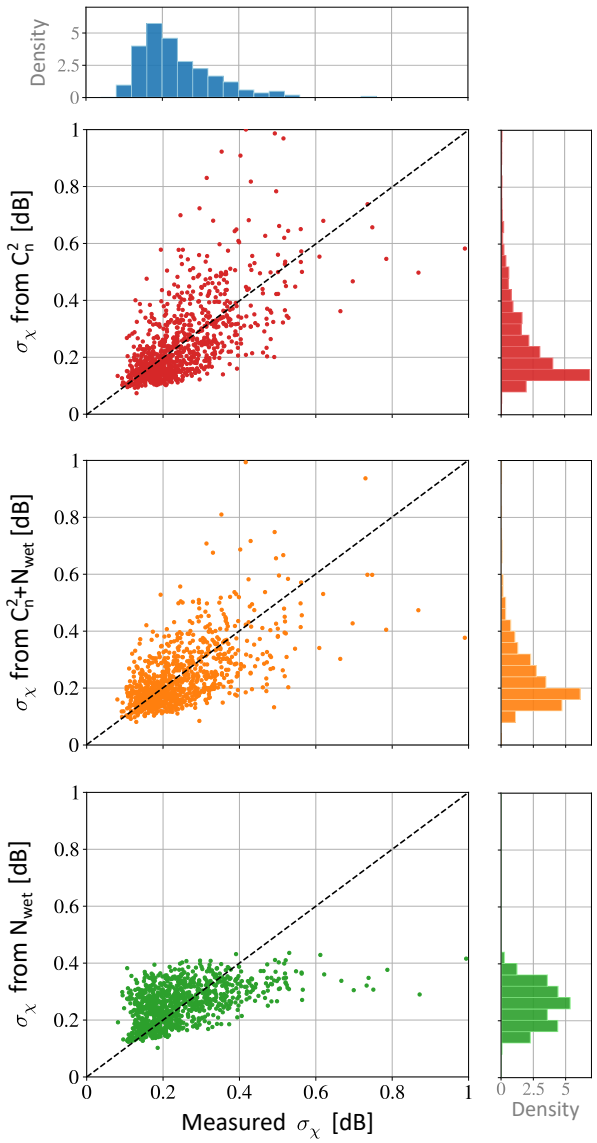

Fig. 5: Correlation plots of σ_χ.

region around the location of interest. This assumption is probably verified at high altitudes, where large atmospheric features are often found, but is questionable close to the ground. Luckily, radiosonde drifting is rather limited in the ground layer, and the turbulent features identified by the radiosonde are probably similar to the ones the communication signal is passing through. Nevertheless, those differences remain to be quantified.

Furthermore, the temporal validity of the predicted C_n^2 profile must also be studied, as turbulence statistics vary in time. Timescales of 10 minutes for the stationarity of turbulence are suggested in the literature [16], that are smaller than the one-hour window used for the scintillation measurements and the 2-hour flight time (on average) of the radiosondes. As a result, varying C_n^2 profiles in space and time could reduce the correlations between the models and the measurements, while

having little or no influence on the distributions.

Validation of C_n^2 profiles is also made difficult by the comparison with measured integrated quantities, such as the scintillation standard deviation. Ideally, measured vertical profiles of C_n^2 should be used to assess the C_n^2 profile model performance.

Finally, all models in this work make use of calibration coefficients, obtained empirically, and further work should assess the validity of those coefficients to other locations.

VI. Conclusion

This work presented two new models (C_n^2 and $C_n^2 + N_{\text{wet}}$ models) for predicting the long-term scintillation standard deviation σ_χ. They have been compared with one year of scintillation measurements at Bjørnøya, and with another model from the literature (N_{wet} model).

All models showed good predictions of the seasonal variations of σ_χ. The new models have been found to provide distributions of σ_χ in excellent agreement with the measured distribution, with correlation coefficients larger than 0.6. They also enabled physical insights about the scintillation standard deviation from the modelled C_n^2 profiles. However, their complexity is larger than traditional empirical models from the literature, and they require high-density radiosonde measurements at the location of interest.

Future work will assess the validity of the hypotheses behind the presented models, as well as their applicability to other locations. As an alternative to radiosonde observations, numerical weather prediction simulations will be considered.

Acknowledgment

The Norwegian Meteorological Institute is thanked for the access to their radiosonde data. Radio propagation measurements at Bjørnøya were funded by ESA Contract No. 4000106010/12/NL/CLP “Ka-band radio characterisation for SatCom services in arctic and high latitude regions”, as well as by Telenor, FFI, UNIK and Norwegian Defence Logistics Organisation (NDLO). The present research is part of the Space4ReLaunch project, which is supported by the SPW Economie Emploi Recherche of the Walloon Region, under the grant agreement No. 2210181.

References

[1] F. S. Marzano, C. Riva, A. Banich, and F. Clivio, “Assessment of model-based scintillation variance prediction on long-term basis using Italsat satellite measurements,” *International journal of satellite communications*, vol. 17, no. 1, pp. 17–36, 1999.

[2] Y. Karasawa, M. Yamada, and J. E. Allnutt, “A new prediction method for tropospheric scintillation on earth-space paths,” *IEEE transactions on antennas and propagation*, vol. 36, no. 11, pp. 1608–1614, 1988.

[3] M. M. van de Kamp, J. K. Tervonen, E. T. Salonen, and J. P. Baptista, “Improved models for long-term prediction of tropospheric scintillation on slant paths,” *IEEE Transactions on antennas and propagation*, vol. 47, no. 2, pp. 249–260, 1999.

[4] ITU-R Recommendation P. 618-13, “Propagation data and prediction methods required for the design of Earth-space telecommunication systems,” *International Telecommunications Union*, 2017.

[5] I. E. Otung, “Prediction of tropospheric amplitude scintillation on a satellite link,” *IEEE Transactions on Antennas and Propagation*, vol. 44, no. 12, pp. 1600–1608, 1996.

[6] H. Vasseur, “Prediction of tropospheric scintillation on satellite links from radiosonde data,” *IEEE Transactions on Antennas and Propagation*, vol. 47, no. 2, pp. 293–301, 1999.

[7] C. Pereira, D. Vanhoenacker-Janvier, N. Jeannin, L. Castanet, and A. Martellucci, “Simulation of tropospheric scintillation on LEO satellite link based on space-time channel modeling,” in *The 8th European Conference on Antennas and Propagation (EuCAP 2014)*, pp. 3516–3519, IEEE, 2014.

[8] F. Quatresooz, D. Vanhoenacker-Janvier, and C. Oestges, “Computation of optical refractive index structure parameter from its statistical definition using radiosonde data,” *Radio Science*, vol. 58, no. 1, 2023.

[9] F. Quatresooz, D. Vanhoenacker-Janvier, and C. Oestges, “Modelling of scintillation at radio and optical frequencies from radiosonde observations,” in *17th European Conference on Antennas and Propagation (EuCAP)*, IEEE, 2023.

[10] M. Rytir, “Ka-band scintillation on low-elevation satellite-earth links in the arctic; long-term measurements and improved modelling,” in *12th European Conference on Antennas and Propagation (EuCAP)*, 2018.

[11] M. Rytir and L. E. Bråten, “Measurements of K-band scintillation on a low elevation satellite-Earth path in Norway,” in *8th European Conference on Antennas and Propagation (EuCAP)*, IEEE, 2014.

[12] B. R. Bean and E. Dutton, *Radio meteorology*, vol. 92. Superintendentof Documents, US GovernmentPrint. Office, 1966.

[13] ITU-R Recommendation P. 453-14, “The radio refractive index: its formula and refractivity data,” *International Telecommunications Union*, 2019.

[14] A. Ishimaru, *Wave propagation and scattering in random media*, vol. 2. Academic press New York, 1978.

[15] V. I. Tatarskii, “The effects of the turbulent atmosphere on wave propagation,” *Jerusalem: Israel Program for Scientific Translations, 1971*, 1971.

[16] H. Vasseur and D. Vanhoenacker, “Characterization and modelling of turbulence-induced scintillation on millimetre-wave line-of-sight links,” in *1995 Ninth International Conference on Antennas and Propagation, ICAP’95 (Conf. Publ. No. 407)*, vol. 2, pp. 292–295, IET, 1995.